Volume 1 | Number 1 | Jan 2013 | Pages 1–100

Journal of
Materials Chemistry A

Materials for energy and sustainability
www.rsc.org/materialsA

ROYAL SOCIETY OF CHEMISTRY

Journal Name

ARTICLE

Enhanced Thermal Shock Resistance of Ultra-high Temperature Ceramic by Biomimetic Surface Modification

Baoxi Zhang,[a] Xinghong Zhang,[a] Yunfeng Qiu,[b] Jiecai Han,*[a] PingAn Hu, *[b] Changqing Hong,*[a] Zujun Peng,[a] Wenbo Han,[a] Guiqing Chen[a] and Ping Hu[a]

Manipulation of heat flow in ceramic matrix composite is of great importance in industrial and academic fields. Energy flow as a typical behavior of heat motion in ceramic surfaces can be confined within specific sites during thermal shock experiments, which weaken temperature gradient distribution, and hence suppress the crack propagation. The heat flow could be rationally controlled by the introduction of nanostructured surface with diverse forced convection coefficient and heat transfer resistance. Taking inspiration from nanofins surface, yttria-stabilized zirconia (YSZ) nanostructures were fabricated using sol-gel method. These bio-inspired coating exhibits high forced convection coefficient (2.884 times) and high heat transfer resistance (30 times) because of the existence of irregular nanowires arrays and porous nanostructure. The introduction of nanostructured coating resulted in rapid depression of the thermal gradient and stress concentration, and the crack propagation was also effectively suppressed. This sol-gel coating method effectively enhanced the thermal shock resistance of ceramic materials, and thus might paves a promising way for the applications of ceramics in extreme environments.

Introduction

The zirconium diboride (ZrB_2) ceramic matrix composite have been regarded as advanced thermal protection materials in virtue of their excellent mechanical properties, remarkable corrosion resistance and fracture toughness.[1,2] However, these ceramics always exhibit inevitable limitations of the brittleness when subjected to the conditions of thermal shock.[3,4] This will catastrophically weaken the ceramic strength at high temperature during the working process of ceramic components, and thus eventually lose the thermal protection or mechanics features.

Recently, great efforts have been dedicated to enhance the thermal shock resistance of ceramics by changing surface structure, mechanical properties, and thermal conductivity.[5-8] She et al. found that the critical temperature difference of porous ceramic for crack initiation strongly dependent on the ratio of fracture strength to elastic modulus. Additionally, the thermal shock behaviour of anisotropic porous ceramic is better than that of isotropic porous ceramic.[9] Collin et al. demonstrated that the fracture toughness was of great importance to the crack growth, which is governed by the combination of residual and thermal stress.[10] According to established theory, the effective thermal conductivity of a reinforced composite will be greater than that of the pristine matrix. However, these improvements can not satisfy the high requirements of space vehicle. Very recently, Song et al. demonstrated that the introduction of a thin air layer at the interface would enhance the thermal shock resistance by surface modification.[11] Taken together, surface modification strategy has been proved to be the most effective way to enhance the thermal shock resistance of ceramics among all the reported methods.

Ceramic membranes have drawn much attention in recent years due to their important properties, especially in high temperature environments such as thermal insulating, thermal matching and corrosion. The designed yttria-stabilized zirconia (YSZ) coatings, which have low heat transfer coefficient and low thermal expansion coefficient, have been studied as a promising material for high-temperature stability and unvaried thermal diffusivity when the temperature is equal or below 900 °C.[12,13] Effective thermal conductivity of porous zirconia (ZrO_2) ceramic was lower than that of the solid matrix due to their two-phase system constituted by a dense solid skeleton and air.[14] Thermal stress mismatch between matrix and coating are extensively investigated owing to their differently Poisson's ratio, Young's modulus, coefficient of thermal expansion and other parameters.[15,16] Hence, the fabrication of YSZ coating may be a practical method to improve thermal shock resistance of ZrB_2 ceramic matrix composite.

As is known, nature contains amazing hierarchical structures with extreme anti-wetting properties, such as a lotus leaf, which provides bio-inspired solutions for solving long-term challenges in materials science. For instance, hydrophobic surfaces can be achieved by the introduction of patterned surface geometries, even when the material surface is intrinsically hydrophilic.[17,18]

Such patterned structures could arrest water from penetrating the cavities on account of capillary forces, making a functional composite interface between the air and the solid surface.[11] Taking advantage of the high water contact angle (CA) and low contact angle hysteresis (CAH), hydrophobic surfaces can be produced, and thus utilized as a versatile platform for the microfluidic management or enhancement of ceramic thermal shock resistance.

Additionally, apart from the introduction bio-inspired hydrophobic surface on the surface of ceramics, some efforts have been devoted to obtain a thermally stable porous surface by self-assembly or micelle aggregation methods.[19] The discovery of mesoporous silica has boosted the formation of porous ceramic materials by liquid-crystal 'templating' mechanism.[20] These template methods can be used to prepare inorganic porous materials regardless of the compatibility between precursor and copolymer templates. Self-assembled organic surfactants were utilized as stabilizing agents to tune the structure of inorganic solids, such as amphiphilic block copolymers.[21,22] These procedures create microscopic domains of phase-separated components between organic and inorganic constituents, and the organic space fillers can be removed by calcination in atmosphere. Mesoporous ZrO_2 was regarded as a promising material in virtue of its thermally stability, large surface area, and high porous volume.[23] Taking all reasons into account, the introduction of bio-inspired hydrophobic surface and porous structure on the surface of ceramics might enhance their thermal shock resistance due to the modulation of heat flow at interface. However, only few related studies were reported on this topic and removal of the organic template at high temperature calcination might cause membrane collapse due to phase transformation, crystal growth and thermal mismatch.

Herein, we present a facile sol-gel method for the fabrication of hydrophobic YSZ membrane with mesoporous nanostructure and irregular nanowires arrays on a ZrB_2 ceramic matrix composite surface. The hydrolysis and condensation process of YSZ precursor could be readily controlled during sol-gel process. Surface properties and porous structure were investigated by means of spectral and microscopic measurements. Thermal shock experiments were also conducted in underwater environments, and a tentative mechanism of present system was proposed.

Experimental

Preparation of YSZ gels

Zirconium oxychloride octahydrate ($ZrOC_{12}\cdot8H_2O$, 99%) and yttrium (III) nitrate hexahydrate ($Y(NO_3)_3\cdot6H_2O$, 99.8%) were purchased from Sigma-Aldrich (Germany). Polyethylene glycol (PEG400, average molecular weight of 400) and absolute ethyl alcohol (EtOH) were obtained from Guangfu Chemical Industry Research Institute (China). In a typical synthesis, a micellar solution containing $ZrOCl_2\cdot8H_2O$, $Y(NO_3)_3\cdot6H_2O$, PEG400 and deionized water was prepared by mixing them with a weight ratio of 4 : 0.383 : 1.776 : 10.136 : 10, respectively. Subsequently, the fluids were hydrolyzed at 60 ºC under stirring for 8 h, and the final mixture became viscous. The resulted composite containing YSZ precursor was placed for 24 h at room temperature.

Preparation of YSZ films

The micro-sized YSZ films were fabricated by dip-coating method. The as-prepared specimens were treated by immersing it in a hot aqueous solution of concentrated ammonia ($NH_3\cdot H_2O$) and hydrogen peroxide (H_2O_2) with a weight ratio 7 : 3 for 1 h at 90 ºC, and washed with deionized water. Then, the as-obtained samples were put into YSZ gels for 10 min, and dragged out with 1 cm/s. Subsequently, the resultant samples were thermally treated for 20 min at 90 ºC in a quartz tube. Calcination was carried out by slowly ramping up temperature to 600 ºC, and maintained at this temperature for 5 h in the air. Dip-coating and calcination of each batch were repeated for 3 times.

Characterization of YSZ films

The morphology and structure of the nanostructure film were characterized by a focusing ion/electronic double beam micro electron microscopy (FIB/SEM, HELIOS NanoLab 600i, FEI, USA) and transmission electron microscope (TEM, Tecnai G^2 F30, FEI, USA). Prior to increase surface conductivity, the samples were coated with thin gold films under vacuum conditions using a precision etching coating sputter (PECS™ 682, Gatan, USA). The crystallinity of the samples after annealing treatment was measured using an X-ray diffractometer with Cu target (XRD, Empyrean, Panalytical, Netherlands). Thermal behavior of the as-prepared YSZ powders was analyzed with thermogravimetric and differential scanning calorimetry (TGA-DSC, SDTA600, TA, USA). The nanoporous character of YSZ film was characterized by N_2 adsorption-desorption isotherms (QuadraWin, Quantachrome, USA). The static contact angles were measured at ambient temperature using a hydrophobicity instrument (JC2000D5, China). Measurements were performed five times to calculate the mean apparent contact angle. Volumes of the droplets were 1.0 μL. The contact angles were measured with a camera after the droplet had been rested on the surface for 2 s.

Mechanical characterization

Ceramic specimens were first cut into 3 × 4 × 36 mm bars with wire-electrode cutting at the ambient temperature. The arc diameter of edge was 0.1 mm. The samples were heated to a preset temperature with a rate of 10 ºC/min, and then were aged at this temperature for 10 min. The heated sample was dipped into deionized water at the room temperature. The residual flexural strength of samples were performed at a nominal displacement rate of 0.50 mm/s until failure during monotonic three point bending experiments, and the values reported were the average of five samples at ambient temperature.

Results and discussion

Biomimetic YSZ coating preparation

Large-scale well-defined functional surface can be fabricated via the sol-gel approach, and the hydrophobicity of as-prepared surface was readily controlled through the modulation of surface composition and nanostructures. It has been reported that 3D bionic nanostructure were realized by the introduction of inverse micelles, the regulation of solvent effects and the condensation of inorganic precursors. Additionally, the pretreatments of substrates with micro-scale topographic features and hydroxyl bonds play important role for enhancing the affinity between colloidal sol and ceramic matrix composite. Fig. 1 is the schematic illustration of preparation

and surface treatment for the construction of YSZ nanostructure. The formation of hydroxyl bonds between colloidal sol and ceramics and thin layer of ZrO_2 are regarded as two effective ways to solve the thermal and mechanical stability of these surface-coated YSZ layers.
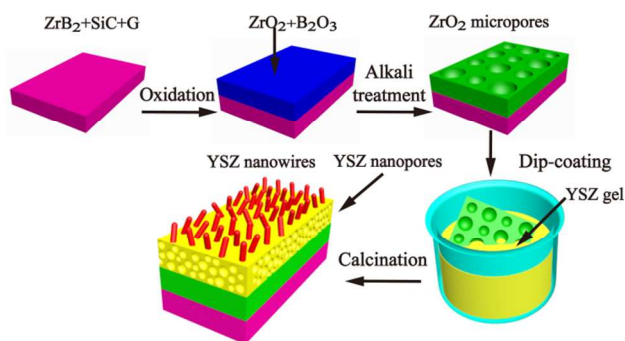
Fig. 1 Schematic illustration of preparation and surface treatment for constructing YSZ nanostructure.

As depicted in Fig. 1, a thin layer of ZrO_2 film with irregular micro-sized pores on ceramic surface was first prepared by oxidation and alkali treatment of the ZrB_2 ceramic matrix composite. PEG400 and absolute EtOH were applied to trigger the nucleation and precipitation process of $ZrOCl_2 \cdot 8H_2O$ and $Y(NO_3)_3 \cdot 6H_2O$, and slow down the growth of gel particles. Meanwhile, strong hydrogen bonding interaction between alcoholic hydroxyl groups and ZrO_2 will facilitate the deposition of coating materials on the surface of ceramic. During the growth process, microscopic phase-separated components occurred between organic and inorganic components generated conformational entropy and steric repulsion. The YSZ sol successfully self-assembled into a supermolecular film with nanopores on the ceramic surface. The thickness of the solution membrane on the sample, which is stipulated by the capillary number (Ca) with $Ca = \eta v / \gamma$, is affected by the viscosity and the concentration of the solution (η), draw out velocity (v) and surface tension (γ).[24]

The SEM image of ZrB_2 ceramic matrix composite is depicted in Fig. 2a. The pretreated surface of ZrB_2 ceramic matrix composite by oxidation at 900 °C is exhibited in Fig. 2b and the thickness of oxide layer is about 20 μm (Fig. S1). It has been confirmed that the composition of the oxide layer are ZrO_2 and amorphous boron oxide (B_2O_3), which was reported by Li and co-authors.[25] B_2O_3 can be removed by alkali etching. The irregular micro-sized pores generated by alkali etching of the ZrB_2 ceramic matrix composite are characterized by SEM. The average diameter of pores is about 2~3 μm shown in Fig 2c. An epitaxial buffering layer composing of microporous structural features could enhance interfacial adhesion and mediate its thermal expansion between coatings and matrix materials, which agree well with previous reported lattice mismatches.[26] The typical SEM images of the surface of substrate in the first and second round after dip-coating and subsequent calcination at 600 °C are presented in Fig. S2a and S2b, respectively. It is clear to see that the surface became smooth, and contained some irregular nano-sized assemblies. We further conduct another round of dip-coating and calcination to produce a nanostructure with nanowires on the surface and nanopores inside the coating. The optical image of YSZ coating after triple round of dip-coating and calcination is illustrated in Fig. 2d. As

shown in Fig. 2e, the surface comprises of YSZ nanowires. It is observed that the average diameter, height and spacing of distributed nanowires are about 30 nm, 200 nm and 100 nm, respectively. The average thickness of YSZ coating is 20 μm (detailed information is provided in Fig. S1).
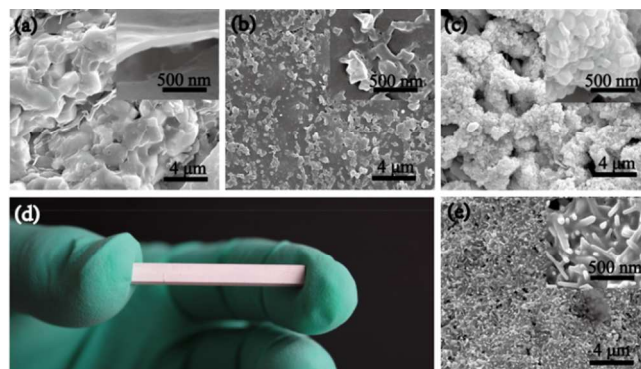
Fig. 2 Surface SEM morphology and optical image of prepared smart YSZ membrane. (a) The SEM image of ZrB_2 ceramic matrix composite; (b) Typical SEM image of ZrB_2 ceramic matrix composite heated at 900 °C for 1 h; (c) The cross-sectional SEM image of sample (b) was treated by immersing it in concentrated $NH_3 \cdot H_2O$ and H_2O_2 at 90 °C for 1 h; (d, e) The optical image and the typical top SEM image of the smart membrane consisting of ZrO_2 nanopores and nanowires after triple dip-coating and calcination at 600 °C, respectively.
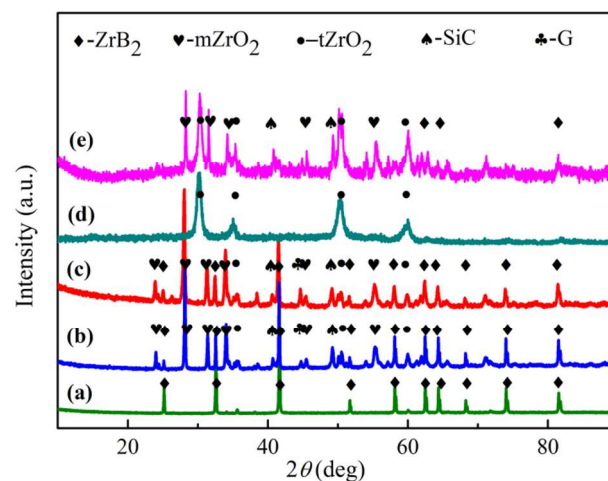
Fig. 3 XRD patterns of matrix material (a), oxidation at 900 °C for 1 h (b), alkali treatment with concentrated $NH_3 \cdot H_2O$ and H_2O_2 at 90 °C for 1 h (c), YSZ powders for 600 °C heat-treatment temperatures (d) and specimens with YSZ coating (e).

XRD results in Fig. 3a confirmed that the matrix material is composed of ZrB_2, silicon carbide (SiC) and graphite (G). As seen in Fig. 2b and 2c, the ceramic surfaces after oxidation at 900 °C and alkali treatment are both composed of tetragonal ZrO_2 and small amounts of monoclinic ZrO_2. The precursor powders showed good crystallization on the ZrB_2 ceramic matrix composite. It is notable that the composite exhibits a broadened peak at ca. 30° in Fig. 3d, which can be identified as

the (111) plane of tetragonal ZrO_2. Further, no monoclinic phase in ZrO_2 powders was observed when sintered under the same conditions. These results demonstrate that our synthetic method restrains the phase transformation from metastable tetragonal phase to monoclinic phase. Consequently, tetragonal ZrO_2 was stabilized by yttrium oxide (Y_2O_3), which agrees well with the conclusion reported by Cao et al.[21]

TEM images for YSZ in Fig. 4a stated that a three-dimension disordered pore structure and the average diameter of nanopores was less than 30 nm. The corresponding selected area electron diffraction (SAED) pattern and a HR-TEM image in Fig. 4b illustrate that the structure consisted of many small polycrystalline YSZ particles with sizes of ca. 20 nm. The interplanar spacing of 0.2995 and 0.2635 nm determined from the HR-TEM image correspond to the (101) and (002) lattice plane of YSZ, respectively. They are consistent with XRD results.

TEM image of the calcinated YSZ powders in Fig. S3a illustrates that YSZ nanocrystallites can be confirmed by their dark contrast. The corresponding SAED pattern in the inset of Fig. S3a illustrates that the structure was assembled by a large amount of polycrystalline YSZ with sizes of about 20 nm. We also found that YSZ nanoparticles lost their regular self-assembled arrangement as depicted in the TEM images owing to the sonication of the sample before the TEM measurement. In addition, A HR-TEM image in Fig. S3b exhibits the high crystallinity of the YSZ with well-defined lattice planes.
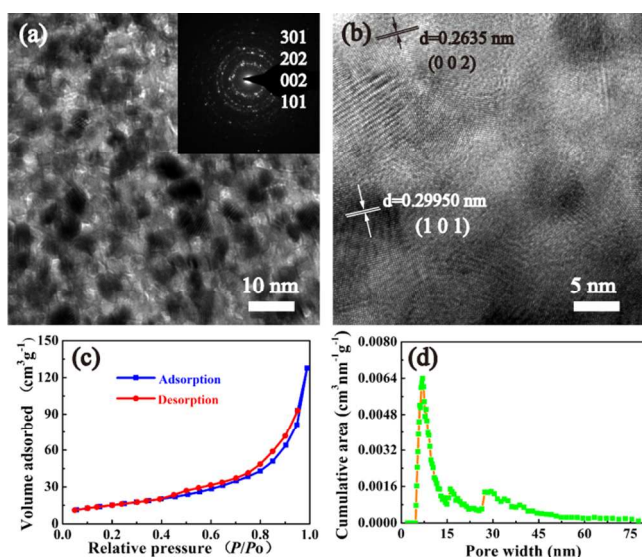
Fig. 4 TEM images of mesoporous YSZ membrane and N_2 sorption analysis. (a) TEM image of the YSZ powders, inset is the SAED pattern taken from the same area; (b) HR-TEM image of YSZ powders; (c, d) N_2 adsorption-desorption isotherms of YSZ powders and the corresponding DFT pore size distribution curve, respectively.

YSZ powders exhibit a type IV isotherm with H3 hysteresis loop in Fig. 4c, which is the typical characteristic of mesoporous YSZ ceramic materials. The respective pore volume and surface area are 0.138 cm^3g^{-1} and 49.266 m^2g^{-1}, which are fundamental to determine the pore size distribution. The pore size distribution of YSZ powder in the range of 2.1~43.0 nm was performed using the density functional theory (DFT), as depicted in Fig. 4d.

The total weight loss of 25% agrees well with the deposition of water below 150 ºC as depicted by the TG curve in Fig. S4. Additionally, there is further weight loss due to the oxidation of the PEG400 when the temperature changed from 200 to 400 ºC. One sharp exothermic peak could be also observed in the thermal flow curve. As temperature above 400 ºC, further weight loss of 5% was accompanied by another exothermal peak in the thermal flow curve due to the formation of the tetragonal YSZ.

The dip-coating treatment produces hierarchical structure with certain roughness and nano-sized surface which greatly affects the physical and chemical properties of the ceramic matrix. 1 μL of distilled water drop is vertically attached on YSZ membrane, and it is found that pronounced Cassie-Baxter wetting in virtue of staying was stable for a long time.[28] The apparent contact angle is 125º for YSZ membrane, whereas the static contact angle is 39º for ceramic sample without membrane (Fig. S5). The Cassie-Baxter wetting regime clarifies that a water droplet is supported partially by YSZ nanostructures and partially by air. In particular, it generates the hydrophobicity of the ceramic surface. It is worth noting that hydrophobicity was created on an intrinsically hydrophilic surface, and it has a vital impact on the manipulation of functional properties of the membrane.

The special hydrophobic properties of 3D hierarchical structures could be demonstrated by the wetting theories for a liquid drop on YSZ membrane. A composite surface of air and heterogeneous membrane is formed in the Cassie−Baxter state, which could be estimated as:[29]

$$\cos \theta^c = f(\cos \theta + 1) - 1 \qquad (1)$$

where, θ^c is the apparent contact angle on a composite surface, θ is the equilibrium contact angle for a flat surface, and f is the area fraction of the solid surface in contact with the liquid. The contact angle of a water drop is dependent on the ratio of area of entrapped air to the area fraction of the nanoscale surface.[30] Hence, a nanoscale rough YSZ surface, containing small air pockets, allows for a decrease in the solid–liquid contact area and maintaining the composite interface, while the small ones enhance the hydrophobicity of the surface. A further exploration of nanoscale roughness on wetting requires the survey of the hierarchical nature, such as lotus leaf.

Evaluation of thermal shock

Recently, the poor thermodynamics robustness of the smart surface under a huge temperature gradient becomes a vital obstacle in practical applications. The biomimetic surface of the solids is designed to enhance the resistance to the matrix material surface cracking. Considering the hydrophobic properties of a smart YSZ membrane, we tend to examine the enhanced resistance of smart surface utilizing the water-cooling method. There are some micro-cracks appears on the coating at 420 ºC in Fig. 5a. More micro-cracks are observed from cross-sectional morphology of the YSZ coating when the temperature is up to 820 ºC in Fig 5b. Thus, vertical cracks of coatings afforded stress relaxation and strain tolerance due to the thermal gradients and thermal expansion mismatch during the quenching process. Crack density, width and depth increase with the actual temperature rising (from 420 ºC to 820 ºC). A massive collapse of the coating was observed at 920 ºC in Figure 5c and 5d. The formation of micro-cracks are completely stochastic and undesirable in virtue of initiation from random defects during processing, however, the smart coating would manage the dynamic effects of the temperature

and thermal stress of ceramic materials. Consequently, the temperature gradient is transparently reduced on the surface of ZrB_2 ceramic matrix composite (L_1 region in Fig. 5f) and YSZ coatings come off substrate, owing to their interfacial stress of thermal expansion mismatch.
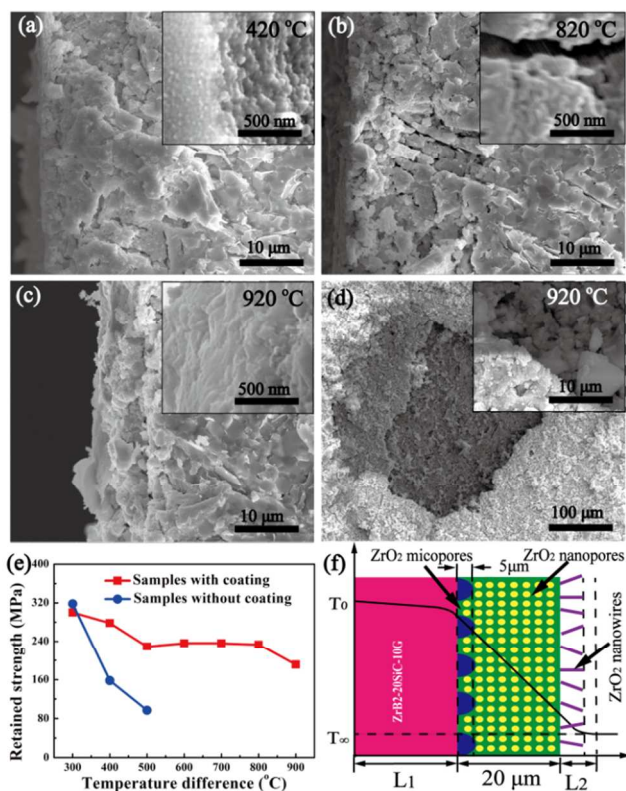
Fig. 5 Thermal shock properties of samples with smart YSZ membrane. (a, b, c) The cross-sectional SEM images of smart membrane collapse quenched in ambient temperature water after heated at 420 ℃, 820 ℃ and 920 ℃ for 10 min, respectively. (d) SEM image of the surface of smart membrane collapse at 920 ℃. (e) The residual flexural strength of ZrB_2 ceramic matrix composite with and without smart membrane along with the difference temperatures. (f) Schematic illustration depicts the temperature distribution at the interface between the solid with YSZ film of nanostructure and water during quenching.

We further detect the residual flexural strength of the specimens with the heterogeneous structures after thermal quenching. Regarding the samples with biomimetic YSZ nanostructures, the retention rate of the residual flexural strength remains approximately 93%, whereas the samples without YSZ nanostructures, a substantial downgrade appears when the temperature is up to 420 ℃ and that only remains 50%. The retention rate of the residual flexural strength maintains about 78% before the temperature over the threshold of 820 ℃, which is markedly higher than unprepared samples. YSZ nanostructured coating spalls from the ceramic substrate due to high tensile shear stress when the thermal shock temperature difference up to 920 ℃, as depicted in Figure 5c and 5d. The cracks perpendicular to the surface of YSZ coating are easily produced by the large temperature gradient difference, owing to the thermal expansion mismatch between coating and substrate. However, the strength retention rate after nanostructured surface treatment maintains approximately three times higher than that of untreated ceramic surface (i.e., only about 25% retention rate quenched at 500 ℃ and 75~78% retention rate even at 820 ℃ without and with smart membrane, respectively), which is also much higher than that in open literatures.[3]

The importance of nanowires and nanopores on the ZrB_2 ceramic matrix composite could be elucidated by the schematic illustration in Figure 5f. During thermal quenching, the immersion of condensed water vapor into the nanowires and nanopores is suppressed at air interface due to the hydrophobic effect of the nanometer structures. The aqueous vapor attachment and transport in porous medium are essentially depended on not only the surface property but also the porous nanostructure due to the resistance effect involved. If the water drops and bubbles are emerged at the inside of the surface channel, the YSZ coating would result in unfavorable nano-channel buttering, and the isolating and resisting effect was also deteriorated. However, the heat flow during quenching are blocked at the nanoporous structure and the thermal transfer is impeded in the bulky ZrB_2 ceramic matrix composite. Therefore, it is assumed that the YSZ nanostructured coating create a thin air layer enveloping between the water and the interior of matrix materials and increase the forced convection coefficient, making the matrix materials insensitive to thermal shock during quenching.

To understand the thermal buttering and blocking effect of the nanostructured surface during thermal shock, it would be essential to comprehend the stress response in smart YSZ membrane. Generally, strain is uniformly distributed across the membrane and declines away from their interface. If the film thickness is appropriate adequately, the introduction of stress accounts for the induced elastic energy relaxation of the associated strain at the interface between the epitaxial film and substrates, which was analogous to dislocation theory in crystal material.[31,32] These stresses are accompanied by abundant local strain fields and swiftly migrate towards the surface at the microscale.[33,34] Consequently, it creates the observed positive strain gradient at the oxide/oxide interfaces, which is analogous to Andrew Pratt reports.[35] So the coupling effect of the Surface-Step-Terrace dimension and stress misfit has an immense impression on the physical properties of epitaxial oxide thin films.[36] Cracks readily nucleate from preferential sites inevitably presented in the as-prepared YSZ membrane and other inherently internal defects.

To further explore the peculiarities of thermal flow in heterogeneous membranes, the heat intensity distributing at the interface as depicted in Figure 5f. Note that most of the thermal gradient is concentrated at the interface between the ceramic matrix and water during quenching. It allows that such thermal buttering effect is evidently different from that without surface nanostructured ceramic materials. The nano-sized roughness and a large amount of air pockets of the YSZ coating have a crucial role in arresting water leakage from the open nanopores. It apparently decreased the contact area between the water and 3D ceramic matrix surface and achieves underwater hydrophobicity. The effective conductivity of the nanostructure is evidently lower than that of the dense bulk YSZ in virtue of the gas in the pores when its size is below 10 μm,[14] so the protective YSZ coating vastly enhance the thermal convection resistance at the interface with a thin air layer. The dynamic effect of temperature and thermal stress, emerging on the surface of the matrix material, are rapidly depressed during thermal shock.

Numerical calculation of thermal shock

A two-dimensional, transient-state forced convection model is performed to estimate the temperature field and the stress distribution. Matrix materials and YSZ coating are isotropic and linearly elastic. External surfaces are subjected to external forced convection from water. The actual surface area composed of YSZ nanowires (A_e) increased greatly to 2.884 times (A) and the forced convection coefficient ($h_e = (A_e/A)\,h$), which is proportional to the actual surface area of sample (A_e), increased to 2.884×10^4 $W \cdot m^2 \cdot K^{-1}$ (h =1×10^4 $W \cdot m^2 \cdot K^{-1}$ for ceramic without coating).[37,38] The thermal expansion coefficient values of substrate at 303 ºC and 594 ºC are 4.74 $K^{-1} \cdot 10^{-6}$ and 5.99 $K^{-1} \cdot 10^{-6}$, respectively. The thermal expansion coefficient values of YSZ coating is 10 $K^{-1} \cdot 10^{-6}$.
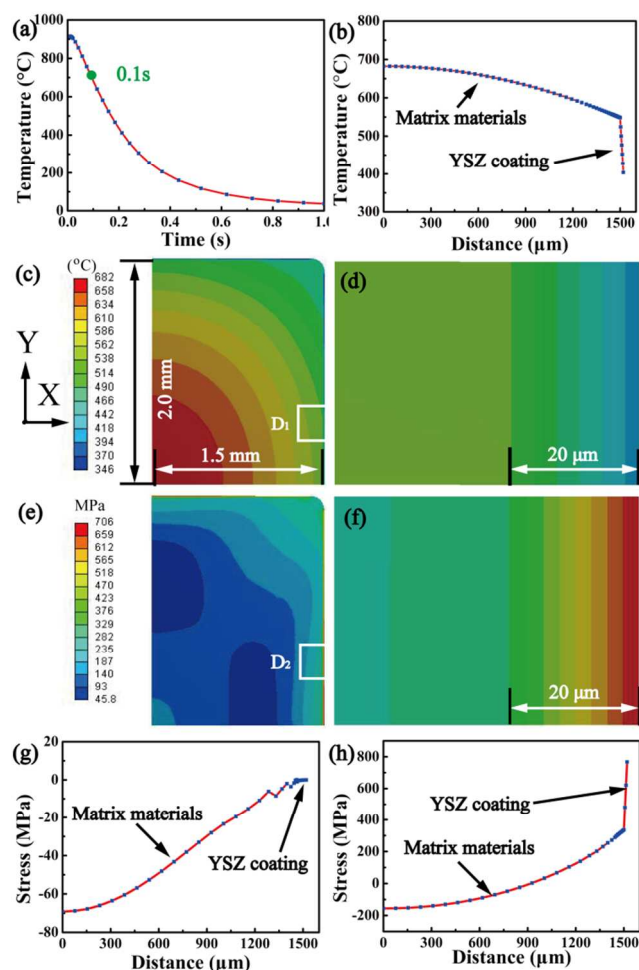
Fig. 6 Numerical simulation predicts the temperature fields and stress distributions. (a) Surface temperature distributions of YSZ coating in thermal shock calculation; (b) Temperature distribution curve through the thickness of coating and substrate in X direction (selected D_1 region); (c, d) Temperature distributions diagram generated in substrate with YSZ coating and local domain of YSZ coating at 0.1 s; (e, f) Stress distributions diagram generated in substrate with YSZ coating and local domain of YSZ coating; (g, h) Stress distribution curves through the thickness of coating and substrate in X and Y direction, respectively (selected D_2 region).

The temperature distribution and thermal stress generated in the substrate and YSZ coating are investigated by finite element analysis. We selected the analysis time at 0.1s (Fig. 6a) to accurately illustrate their actual response. As depicted in Figure 6b, the temperature field notably descend from 550 ºC to 410 ºC at the nanostructured YSZ layer and remains invariably through the substrate. The temperature distributions generated in substrate with YSZ coating and local region of YSZ coating are exhibited in Fig. 6c and 6d, respectively. It is observed that large temperature gradient mainly distribute across the YSZ coating (Figure 6b). The results of simulated thermal stress distribution diagram in substrate and local region of YSZ coating are depicted in Fig. 6e and 6f, respectively. It is found that the thermal stress in YSZ the coating is higher than that in substrate (336 MPa) due to the effect of temperature gradient and the thermal mismatch between YSZ coating and substrate. The tensile stress of coating surface in Y direction depicted in Fig. 6h reaches to 767 MPa, which is dramatically higher than that in X direction (about 0 MPa). It demonstrates that crack propagation of energy dissipation is along X direction (D_2 region), which agree well with thermal quenching experiments (Fig. 5a, 5b). Hence, the energy dissipation of thermal shock was confined within YSZ coating and stress concentration had been suppressed. These results illustrate that we could impressively reconstruct the thermal shock surface of ceramic materials by the diverse dynamic effect of temperature and thermal stress distribution.

Conclusions

The integration of sol-gel technology and a heterogeneously epitaxial growth approach leads to the facile preparation of biomimetic nanostructure of YSZ, which was applied as functional surface for modulating the geometrical parameters and wettability. The as-prepared smart coating layers could resist water and enhance forced convection coefficient of the interface due to the rough surface and the trapped air layer formed at solid/liquid interface. The dynamic effect of temperature and thermal stress, emerging on the surface of ZrB_2 ceramic matrix composite, are rapidly depressed. It ultimately restrains the crack propagation in thermal shock process. These self-localized entities exhibit high forced convection coefficient and high heat transfer resistance, depending on the synergistic effect of the nanorod arrays surface and the introduction of mesopores. Matrix materials eventually have less cracks and deleterious damage because YSZ coatings bear stress and thermal energy from temperature gradient and thermal expansion mismatch. Present method might develop a promising way to solve the knotty mechanical behaviours of ceramic materials under thermal shock effect.

Acknowledgements

Notes and references

[a] Science and Technology on Advanced Composites in Special Environments Laboratory, Harbin Institute of Technology, Harbin, Heilongjiang, 150080, P. R. China

[b] Key Lab of Microsystem and Microstructure, Harbin Institute of Technology, Ministry of Education, No. 2 YiKuang Street, Harbin, 150080, P. R. China

1 A. L. Chamberlain, W. G. Fahrenholtz and G. E. Hilmas, J. Am. Ceram. Soc., 2004, **87**, 1170-1172.

2 W. G. Fahrenholtz, G. E. Hilmas, I. G. Talmy and J. A. Zaykoski, J. Am. Ceram. Soc., 2007, **90**, 1347-1364.

3 Z. Wang, C. Hong, X. Zhang, X. Sun and J. Han, Mater. Chem. Phys. 2009, **113**, 338-341.

4 T.-H. Lee, J.-H. Sun, H. H. Nersisyan, H.-G. Jung, K.-H. Lee and J.-H. Lee, Composites: Part A, 2012, **43**, 1490-1496.

5 J. Xinxin, Z. Xinghong, H. Jiecai, H. Ping and H. Rujie, Mater. Sci. Eng. A, 2013, **588**, 175-180.

6 G. Ziegler, Z. Werkstofftech 1985, **16**, 45-55.

7 J. Francl and W. D. Kingery, J. Am. Ceram. Soc., 1954, **37**, 99-107.

8 P. Zhou, P. Hu, X. Zhang and W. Han, Scripta Mater., 2011, **64**, 276-279.

9 J. She, J.-F. Yang, D. D. Jayaseelan, N. Kondo, T. Ohji and S. Kanzaki, J. Am. Ceram. Soc., 2003, **86**, 738-740.

10 M. Collin and D. Rowcliffe, Acta Mater., 2000, **48**, 1655-1665.

11 F. Song, S. Meng, X. Xu and Y. Shao, Phys. Rev. Lett., 2010, **104** (125502), DOI: 10.1103/PhysRevLett.104.125502.

12 M. Ogawa, Heat Transfer-Asian Research 2008, **37**, 57-67.

13 D. R. Clarke, Surface and Coatings Technology 2003, **163-164**, 67-74.

14 B. Nait-Ali, K. Haberko, H. Vesteghem, J. Absi, D. S. Smith, Journal of the European Ceramic Society 2006, **26**, 3567-3574.

15 Y. Islamoglu, E. Celik, C. Parmaksizoglu, Y.S.Hascicek, Materials and Design 2002, **23**, 531-536.

16 V. Chawla, R. Jayaganthan, R. Chandra, Journal of Materials Processing Technology 2008, **200**, 205-211.

17 L. Feng, S. Li, Y. Li, H. Li, L. Zhang, J. Zhai, Y. Song, B. Liu, L. Jiang and D. Zhu, Adv. Mater. 2002, **14**, 1857-1860.

18 C. Dorrer and j. Rühe, Adv. Mater., 2008, **20**, 159-163.

19 B. T. Holland and C. F. Blanford, A. Stein, Science, 1998, **281**, 538-540.

20 C. T. Kresge, M. E. Leonowicz, W. J. Roth, J. C. Vartuli and J. S. Beck, Nature, 1992, **359**, 710-712.

21 H. f. Zhang, G. C. Hardy, M. J. Rosseinsky and A. I. Cooper, Adv. Mater., 2003, **15**, 78-81.

22 K. Nakanishi, Y. Kobayashi, T. Amatani, K. Hirao and T. Kodaira, Chem. mater. 2004, **16**, 3652-3658.

23 E. Liu, A. J. Locke, W. N. Martens, R. L. Frost and X. Yang, Cryst. Growth Des., 2012, **12**, 1402-1410.

24 Y. Chen, L. Wang, Y. Xue, L. Jiang and Y. Zheng, Sci. rep., 2013, **3**, 2927, DOI: 10.1038/srep02927.

25 N. Li, S. Zhou, X. Jin, P. Hu, P. Wang. J. Alloys Compd., 2015, **620**, 142-148.

26 K. J. Franke, P. Gille, K.-H. Rieder and W. Theis, Phys. Rev. Lett., 2007, **99**, 036103, DOI: 10.1103/PhysRevLett.99.036103.

27 F. Cao, Y. Gao, H. Chen, X. Liu, X. Tang and H. Luo, J. Solid State Chem., 2013, **202**, 168-172.

28 M. Nosonovsky, Langmuir, 2007, **23**, 3157-3161.

29 A. B. D. Cassie and S. Baxter, Trans. Faraday Soc., 1944, **40**, 546-561.

30 L. Gao and T. J. McCarthy, Langmuir, 2006, **22**, 2966-2967.

31 H.-J. Gao, C. L. Chen, B. Rafferty, S. J. Pennycook, G. P. Luo and C. W. Chu, Appl. Phys. Lett., 1999, **75**(17), 2542, DOI: 10.1063/1.125071.

32 F. Reichel, L. P. H. Jeurgens and E. J. Mittemeijer, Phys. Rev. B, 2006, **74**, 144103, DOI: 10.1103/PhysRevB.74.144103.

33 B. Gilbert, F. Huang, H. Zhang, G. A. Waychunas and J. F. Banfield, Science, 2004, **305**, 651-654.

34 D. Mordehai, M. Kazakevich, D. J. Srolovitz and E. Rabkin, Acta Mater., 2011, **59**, 2309-2321.

35 A. Pratt, L. Lari, O. Hovorka, A. Shah, C. Woffinden, S. P. Tear, C. Binns and R. Kröger, Nat. mater., 2014, **13**, 26-30.

36 C. Ma, M. Liu, C. Chen, Y. Lin, Y. Lin, J. S. Horwitz, J. Jiang, E. I. Meletis and Q. Zhang, Sci. rep., 2013, **3**, 3092, DOI: 10.1038/srep03092.

37 J. P. Holman, Heat Transfer, McGraw-Hill Education, Beijing, China 2002

38 F. P. Incropera, D. P. DeWitt, T. L. Bergman, A. S. Lavine, Functionals of Heat and Mass Transfer, Wiley, New York, USA 2007.